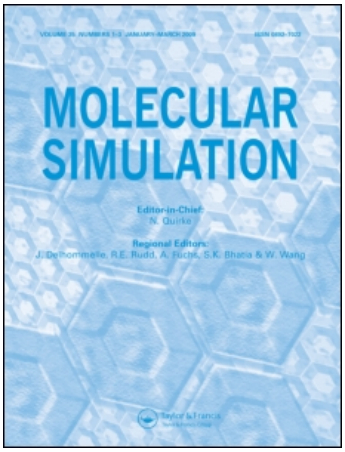


**Molecular Simulation**
Publication details, including instructions for authors and subscription information:
http://www.informaworld.com/smpp/title~content=t713644482

# Brownian Dynamic Simulation of Restricted Molecular Diffusion. The Symmetric and Deformed Cone Models

I. I. Fedchenia[a]; P. -O. Westlund[a]; U. Cegrell[b]
[a] Department of Physical Chemistry, University of Umeå, Umeå, Sweden [b] Department of Mathematics, University of Umeå, Umeå, Sweden

**To cite this Article** Fedchenia, I. I. , Westlund, P. -O. and Cegrell, U.(1993) 'Brownian Dynamic Simulation of Restricted Molecular Diffusion. The Symmetric and Deformed Cone Models', Molecular Simulation, 11: 6, 373 — 393
**To link to this Article: DOI:** 10.1080/08927029308022521
**URL:** http://dx.doi.org/10.1080/08927029308022521

*Molecular Simulation*, 1993, Vol. 11, pp. 373-393
Reprints available directly from the publisher
Photocopying permitted by license only



# BROWNIAN DYNAMIC SIMULATION OF RESTRICTED MOLECULAR DIFFUSION. THE SYMMETRIC AND DEFORMED CONE MODELS

FEDCHENIA I.I., WESTLUND P.-O.

*Department of Physical Chemistry, University of Umeå, Umeå S-90187 Sweden*

CEGRELL U.

*Department of Mathematics, University of Umeå, Umeå S-90187 Sweden*

*(Received December 1992, accepted February 1993)*



Three different algorithms are presented for Brownian Dynamics simulations of diffusion on the unit sphere restricted by the intersection with a symmetric or distorted cone. The second rank time correlation function

$$K_2(t) = \sum_n \langle D^2_{0n}(\theta(t), \varphi(t)) {}^* D^2_{0n}(\theta(0), \varphi(0)) \rangle = \langle 3[\mathbf{n}(t)\mathbf{n}(0)]^2 - 1 \rangle / 2$$

has been determined. The three algorithms are compared and discussed with respect to computational efficiency and accuracy.

KEY WORDS: Brownian Dynamics, Langevin equations, rotational diffusion, quaternions, reorientational correlation functions.

## 1. INTRODUCTION

Restricted diffusion of a unit vector, $\mathbf{n}(\theta(t), \varphi(t))$, specified by the polar angles $\theta$ and $\varphi$, in a cone of semi angle $0 < \theta_b < \pi$ is one of the most frequently used dynamic models to mimic restricted molecular motions in condensed phases. The cone model [1] is simple and may be considered unphysical since the potential is discontinuous at the boundary. However, it can be considered as a good zero-order approximation of the real mean field potential for the interaction between the molecule and the environment.

In this paper we present Brownian dynamic calculations of restricted diffusion in a cone using three different algorithms. We have investigated the time autocorrelation function of second rank spherical harmonics for the cases of restricted diffusion in *symmetric* and *deformed* cones.

The analytical solution of the isotropic diffusion equation in a symmetric cone potential has been presented by Wang and Pecora [2]. They calculated the time correlation functions of first and second rank spherical harmonics for semi-angle

less than $\pi/2$. The probability density $P(\theta, \varphi, t)$ satisfying the restricted rotational diffusion equation was obtained by the method of variables separation. Kumar [3, 4] extended the analytical treatment of diffusion in a symmetric cone and presented analytical solution for the case of anisotropic diffusion. The eigenfunction expansion is particularly useful in paramagnetic nuclear spin relaxation studies [5] and in ESR slow motion line shape calculations [6]. Lipari and Szabo [7–9] have obtained closed form approximations of the integral correlation time of spherical harmonics of the second rank. The main restriction in the analytical treatment is the azimuthal symmetry of the cone, that is, the cone must have $C_\infty$ symmetry around its central axis.

The Brownian Dynamic simulation method gives the explicit dynamic of the "molecule" in the form of trajectories. These are necessary for model calculations in the cases where an eigenfunctions expansion of the probability density or an analytical treatment of the time correlation functions are not possible to obtain. This approach requires less memory compared to the eigenfunction expansion when slow motion ESR line shapes and paramagnetic nuclear spin relaxation rates are to be calculated. The price one has to pay is an increase in CPU time. However, when working with workstations where the memory is limited to 64 Mb or less and the access of CPU time is in principal unlimited the BD simulation technique looks more favorable.

There are four fields of research that have motivated us to apply the BD simulation technique when restricted molecular diffusion is modeled:

(i) The first one is spectroscopic studies of translation motion of lipid molecules on the surface of complicated aggregates, formed by many amphiphilic molecules. In NMR and ESR spectroscopy, spin relaxation is induced by orientational fluctuation of second rank tensorial functions present in the spin-lattice coupling hamiltonian. The characteristic correlation times of the internal molecular motions are generally found to be one or two order of magnitude faster than the translational diffusion motion. This separation of time scales legitimate a partially averaged spin-lattice interaction (NMR) in the coordinate system defined by the $z_D$-axis fixed perpendicular to the interface. Thus, when the molecule diffuses along the curved interface it induces a stochastic time dependence in the orientation of the molecular normal $\mathbf{n}(\theta(t), \varphi(t))$ relative to the laboratory fixed frame $z_L$ and consequently in the residual spin-lattice coupling. The NMR relaxation rates are determined by the second rank correlation function of the form

$$C_n(t) = \langle D^2_{0n}(\theta(t), \varphi(t))^* D^2_{0n}(\theta(0), \varphi(0))\rangle,$$

where $D^2_{0n}(\theta(t), \varphi(t))$ is a Wigner rotation matrix element and $\theta(t)$, $\varphi(t)$ are Euler angles; $\langle \ldots \rangle$ denotes an ensemble average.

This can be determined if we know the diffusion induced orientational fluctuation of the molecular normal $\mathbf{n}(\theta(t), \varphi(t))$ projected on the unit sphere. The relevant mathematical procedure was described by Halle *et al.* [10] in a paper about NMR relaxation in bicontinuous cubic liquid crystals modeled as minimal surfaces. Starting from the force free diffusion equation in terms of the Laplace-Beltrami operator one may define transformations to the $x - y$ plane or unit sphere using the stereographic projection or the Gauss map, respectively. The force free diffusion equation on a general 2D manifold will be transformed to a Smoluchowsky

type of diffusion equation. In this context this is the first in a series of papers devoted to time correlation functions of NMR and ESR relaxation experiments and their relation to the topology of three dimensional surface structures. In particular we are interested in how the geometric structure of bicontinuous lyotropic liquid-crystalline phases is reflected in NMR and ESR relaxation studies.

Our aim in this paper is to investigate different computational algorithms suitable for Brownian Dynamic simulation of orientational diffusion. For the symmetric cone model it is possible to determine the relevant correlation functions analytically. Consequently we are able to determine the computational error accurately for the three different simulation algorithms.

For most of the membrane model surfaces the corresponding diffusion equation on the unit sphere does not have an analytical solution. Diffusion in a distorted cone is an example where no analytical solution is available.

(ii) In fluorescence depolarization studies the fluorescence emission anisotropy $r(t)$ of chromophore pairs incorporated into a macromolecule may give structural information of the mean distance between the chromophore molecules. This method requires that the energy transfer mechanism between donor-donor pairs can be analyzed in the presence of molecular dynamics [11]. The Brownian Dynamic simulation method is a powerful technique for modeling of the mobility of chromophores. Furthermore, great flexibility is available with respect to the choice of dynamic models for internal motion of the chromophores.



(iii) The ESR line shape calculations of liquid crystalline phases. Here the electron spin system of a nitroxide radical bound to the alkyl chain of a lipid molecule residing in a bilayer is found to be in the slow motion regime. It means that the electron spin relaxation takes place in the same time scale as the reorientation of the spin bearing lipid molecule. One has to rest on the eigenfunction expansion of the probability density function which is implemented in the Stochastic Liouville equation [12, 13]. The cone model with a semi angle in the range $0 < \theta_b < \pi$ is an alternative model to the most often used pseudo potentials [12, 13] and has recently been applied to the restricted lipid dynamics in lamellar phase of Lyso Lecithin water systems [4]. Direct simulation of ESR line shapes by means of the stochastic Liouville equation requires explicit calculation of the dynamical motion. An approach of this kind has recently been presented [14].

(iv) Finally, in paramagnetic nuclear spin relaxation theory the problem of including dynamic models in the theoretical treatment of relaxation is similar to that in ESR line shape calculations [3, 15]. The electron spin system may be in the slow motion regime and an eigenfunction expansion of the probability density describing the molecular motion is required. One further complication in this field is the need of a much wider variation of dynamic models which describe the fluctuation of the spin-lattice coupling. As an example we investigate the cone model with semiangles in the range $\pi/2 < \theta_b < \pi$ previously not investigated. This is a relevant extension of the so called pseudo-rotation model used to mimic time fluctuations in the zero-field splitting due to the perturbation of the hydration shell symmetry of a paramagnetic transition metal ion due to water molecule wagging, twisting and rocking motion. When the metal ion binds to macromolecules or membranes this pseudo-rotation becomes restricted [15, 16]. That is, when some

water molecules of the hydration shell are exchanged for other atoms or molecules of the macromolecules. Then the symmetry of the aquo-metal-complex is lowered. This effects the fluctuation of the ZFS interaction and may be incorporated in the pseudo-diffusion model of the ZFS interaction by assuming a symmetric or distorted cone model.

So far we have listed four fields of research motivating this work. The outline of this paper is as follows. In section 2 we formulate the restricted diffusion problem. We present the method to calculate the diffusion on the unit sphere in Cartesian coordinates in section 3. The corresponding 3 dimensional Langevin equation is derived. The quaternion parameterization and the 4-dimensional Langevin equation in Stratonovich interpretation is described in section 4. In section 5 the stereographic projection and a 2-dimensional stochastic equation in Ito form is introduced. Section 6 comprises computational results of the distorted and undistorted cone model. We conclude with a comparison of the different algorithms in terms of error characteristics, precision and computational efficiency. Technical questions concerning the treatment of the boundary conditions in BD simulations can be found in two Appendixes.



## 2. RESTRICTED DIFFUSION IN A CONE

The equation for free diffusion of the unit vector **n** is

$$\frac{\partial P(\theta, \varphi, t|\theta_0, \varphi_0)}{\partial t} = D\,\Delta_{\theta_0,\varphi_0} P(\theta, \varphi, t|\theta_0, \varphi_0) = D\left(\frac{1}{\sin\theta_0}\frac{\partial}{\partial\theta_0}\left(\sin\theta_0\frac{\partial P}{\partial\theta_0}\right) + \frac{1}{\sin^2\theta_0}\frac{\partial^2 P}{\partial\varphi_0^2}\right) \tag{1}$$

where $(\theta, \varphi)$ are polar and azimuthal angles in spherical coordinates.

The cone model refers to the restricted diffusion of the unit vector in a symmetric cone defined by semiangle $\theta_b \in [0, \pi]$. The boundary condition for the symmetric cone is

$$\left.\frac{\partial P}{\partial\theta}\right|_{\theta=\theta_b} = 0 \tag{2}$$

which is independent of $\varphi$ (Figure 1) [2, 8, 9]. Diffusion in a distorted cone is described by equation (1) with the boundary condition

$$\left.\frac{\partial P}{\partial\theta}\right|_{\theta=\theta_b(\gamma)} = 0 \tag{3}$$

The case of restricted diffusion with the boundary condition (2) has been studied analytically in the past [5–9]. All analytical results for solutions of the equation (1) were obtained using separation of variables which is possible only for the boundary condition (2). But even in this case all practically concise results were obtained only for angles $\theta \leq \pi/2$. No analytical results are known for the boundary condition (3).

Brownian dynamics as a numerical method is a natural choice to solve (1) since

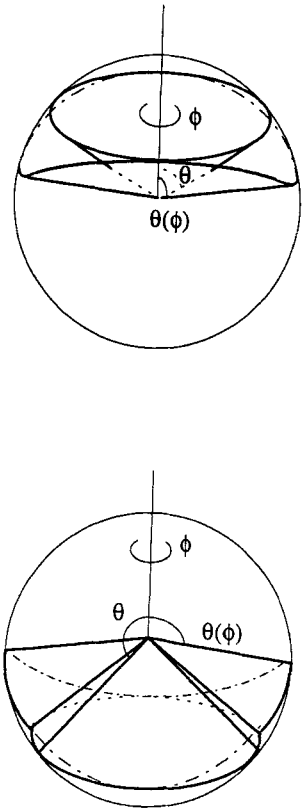


**Figure 1** Undistorted and distorted cone (boundary conditions (2) and (3)). (a) $\theta_b < \pi/2$; (*b*) $\theta_b > \pi/2$.



the more general boundary condition (3) does not cause any additional difficulties in the computational scheme. To the best of our knowledge Brownian dynamics technique has not previously been used to solve equation (1) with the boundary conditions (2) or (3).

In this work we propose three different numerical algorithms to stimulate equation (1) with boundary conditions (2) or (3) and use them to determine the correlation function

$$K_2(t) = \sum_n \langle D^2_{0n}(\theta(t), \varphi(t)) {}^* D^2_{0n}(\theta(0), \varphi(0)) \rangle = \langle 3[\mathbf{n}(t)\mathbf{n}(0)]^2 - 1 \rangle / 2.$$

Here $\mathbf{n}(t)$ is the radius-vector of a diffusing point on the sphere surface.

## 3. THE LANGEVIN EQUATIONS IN CARTESIAN COORDINATES

The general idea of The Brownian dynamic approach is to study the Langevin equations [17, 18] corresponding to equation (1). All correlation functions and

moments can then be obtained as averages of functionals taken on these trajectories. The Langevin equations corresponding to the backward Kolmogorov equation (1) reads

$$\begin{aligned} d\theta &= D\,ctn\,\theta\,dt + D^{1/2}d\mathbf{W}_\theta \\ d\varphi &= D^{1/2}\sin^{-2}\theta\,d\mathbf{W}_\varphi \end{aligned} \tag{4}$$

where $d\mathbf{W}_\theta$ and $d\mathbf{W}_\varphi$ are standard Wiener processes. Evidently they are not very suitable for numerical simulations due to singularities in the $\sin^{-1}\theta$ term.

For the cone model it is possible to accomplish a procedure of imbedding in $\mathbf{R}^3$. Indeed if we take

$$\frac{P(x, y, z, t|x_0, y_0, z_0)}{\partial t} = D\,\Delta_{x_0, y_0, z_0} P(x, y, z, t|x_0, y_0, z_0) \tag{5}$$

and change variables to spherical coordinates we obtain

$$\frac{\partial P(r, \theta, \varphi, t|r_0, \theta_0, \varphi_0)}{\partial t} = D\left\{\frac{1}{r_0^2}\Delta_{\theta_0, \varphi_0} + \Delta_{r_0}\right\} P(r, \theta, \varphi, t|r_0, \theta_0, \varphi_0) \tag{6}$$

here

$$\Delta_{r_0} = \frac{1}{r_0^2}\frac{\partial}{\partial r_0} r_0^2 \frac{\partial}{\partial r_0}$$

$\Delta_{r_0}$ is the radial part of the Laplace operator. For the solution of (6) to coincide with the solution of the original problem (1) we need the equation

$$D\,\Delta_{r_0} P(r, \theta, \varphi, t|r_0, \theta_0, \varphi_0)\,|_{r_0 = 1} = 0 \tag{7}$$

to be satisfied in all time domain. This can be achieved by imposing an additional boundary condition

$$\frac{\partial}{\partial r_0} P(r, \theta, \varphi, t|r_0, \theta_0 \varphi_0)\,|_{r_0 = 1} = 0 \tag{8}$$

which means the absence of probability flux perpendicular to the surface of the unit sphere [17].

We can thus simulate the Langevin equations corresponding to (5) which are extremely simple and free of any singularities

$$\begin{aligned} dx &= D^{1/2}d\mathbf{W}_x \\ dy &= D^{1/2}d\mathbf{W}_y \\ dz &= D^{1/2}d\mathbf{W}_z \end{aligned} \tag{9}$$

A trajectory of the random process in the space of imbedment $\mathbf{R}^3$ which gives the required transient probability density $P(\theta, \varphi, t|\theta_0, \varphi_0)$ is shown in Figure 2. Projection of the final point after every step back to the surface of the unit sphere gives the probability flux which is equal to zero for all time steps. The fact that this process is the diffusion on the surface of the unit sphere was proved in [18 and references therein] in terms of a nonlinear transformation of the standard

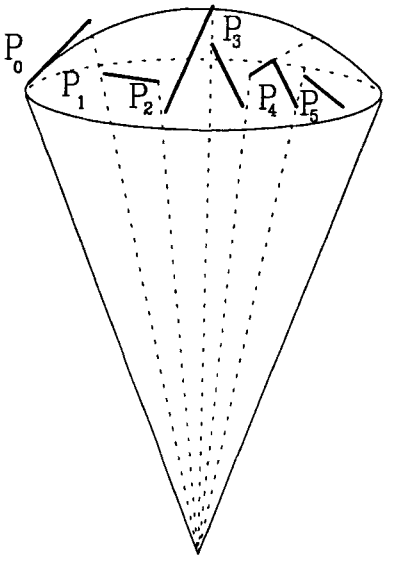


**Figure 2** Trajectories of Langevin equations (9) with projection of the end points in every step back to the surface of the unit sphere. $P_0$, $P_1$ . . ., $P_5$ are situated on the surface and are used as the starting position for the next step.



Wiener process. Our considerations about the probability flux across the surface are very close to those used in [19] and very useful in practical simulations.

The numerical realization of this algorithm consists in the following steps:

1. Starting from a point on the surface of the unit sphere $\{x_i, y_i, z_i;\ x_i^2 + y_i^2 + z_i^2 = 1\}$ which is the resulting position of the previous step i-1 one moves to $\{\tilde{x}_{i+1}, \tilde{y}_{i+1}, \tilde{z}_{i+1}\}$ according to numerical version of (9)

$$\begin{aligned} \tilde{x}_{i+1} &= x_i + D^{1/2}\Delta\mathbf{W}_x(t_i, t_{i+1}) \\ \tilde{y}_{i+1} &= y_i + D^{1/2}\Delta\mathbf{W}_y(t_i, t_{i+1}) \\ \tilde{z}_{i+1} &= z_i + D^{1/2}\Delta\mathbf{W}_z(t_i, t_{i+1}) \end{aligned} \tag{10}$$

where $\Delta\mathbf{W}_{x,y,z}(t_i, t_{i+1}) = h Z_{x,y,z}$; $h = t_{i+1} - t_i$ - is the time step and $\{Z_{x,y,z}\}$ are three standard mutually independent Gaussian deviates (with zero mean value and unit dispersion).

2. $\{\tilde{x}_{i+1}, \tilde{y}_{i+1}, \tilde{z}_{i+1}\}$ is then projected back to the surface of the unit sphere and the coordinates $\{x_{i+1}, y_{i+1}, z_{i+1}\}$ of this point are taken then as the coordinates of the trajectory position at the step $i + 1$.

$$\begin{aligned} x_{i+1} &= \tilde{x}_{i+1}/(\tilde{x}_{i+1}^2 + \tilde{y}_{i+1}^2 + \tilde{z}_{i+1}^2)^{1/2} \\ y_{i+1} &= \tilde{y}_{i+1}/(\tilde{x}_{i+1}^2 + \tilde{y}_{i+1}^2 + \tilde{z}_{i+1}^2)^{1/2} \\ z_{i+1} &= \tilde{z}_{i+1}/(\tilde{x}_{i+1}^2 + \tilde{y}_{i+1}^2 + \tilde{z}_{i+1}^2)^{1/2} \end{aligned} \tag{11}$$

3. One takes $\{x_{i+1}, y_{i+1}, z_{i+1}\}$ as the starting position for the step $i+2$ and repeat the steps 1 and 2.

Now we have to connect boundary conditions (2) or (3) with the behavior of trajectories (9) after they hit the boundary. Such connection seems not to have been established yet for all possible boundary conditions for the Fokker-Planck or the backward Kolmogorov equations. However, from the very elucidative work by Chandrasekhar [20] and the formal mathematical proof of Gikhman and Skhorohod [21] we know that if a trajectory of (9) is rejected from the boundary as it is shown in Figure 3 (angle of incidence is equal to angle of rejection) then the probability distribution $P(\theta, \varphi)$ satisfies boundary conditions (2) or (3). Hence, the most difficult part of the algorithm is the calculation of rejection point after the trajectory has crossed the boundary. A detailed description of this procedure is given in Appendix A.

## 4. QUATERNION PARAMETERIZATIONS

Equation (9) can be interpreted as the Euler-Langevin equation for angular velocity $\omega = (x, y, z)$ of the spherical top which exhibits noninertial motion under the action of random noise $(d\mathbf{W}_x, d\mathbf{W}_y, d\mathbf{W}_z)$. Another possibility to obtain singularity free Langevin equations for the angle variables is the quaternion parameterization which is widely used in calculation of the angular dependence of rigid bodies and molecular motion [22–25].

Quaternion parameters are defined through the Euler angles as

$$\mathbf{q} = \begin{pmatrix} e_0 \\ e_1 \\ e_2 \\ e_3 \end{pmatrix} = \begin{pmatrix} \cos(\theta/2)\cos([\psi+\varphi]/2) \\ \sin(\theta/2)\cos([\psi-\varphi]/2) \\ \sin(\theta/2)\sin([\psi-\varphi]/2) \\ \cos(\theta/2)\sin([\psi+\varphi]/2) \end{pmatrix} \tag{12}$$

and the components of the unit vector $\mathbf{n}$ are

$$\begin{aligned} n_x &= 2[e_1 e_3 - e_0 e_2] \\ n_y &= -2[e_2 e_3 + e_0 e_1] \\ n_z &= e_0^2 + e_3^2 - e_1^2 - e_2^2 \end{aligned} \tag{13}$$

Using equation (9) as a model for random motion of angular velocity the matrix equation for quaternion dynamics is

$$d\mathbf{q} = \mathbf{R}(d\mathbf{W}_{x,y,z})\mathbf{q} = \frac{D^{1/2}}{2} \begin{pmatrix} 0 & d\mathbf{W}_z & -d\mathbf{W}_x & -d\mathbf{W}_y \\ -d\mathbf{W}_z & 0 & -d\mathbf{W}_y & d\mathbf{W}_x \\ d\mathbf{W}_x & d\mathbf{W}_y & 0 & d\mathbf{W}_z \\ d\mathbf{W}_y & -d\mathbf{W}_x & -d\mathbf{W}_z & 0 \end{pmatrix} \begin{pmatrix} e_0 \\ e_1 \\ e_2 \\ e_3 \end{pmatrix} \tag{14}$$

From (12) we have identities

$$e_0^2 + e_1^2 + e_2^2 + e_3^2 = 1 \tag{15}$$

and

$$\mathbf{n}(t)\mathbf{n}(t) = 1 \tag{16}$$

valid for all times. Thus, (15) must also follow from (14). However, $d\mathbf{W}_{x,y,z}$ enter (14) in a parametric way and, consequently, the solution of (14) depends on the interpretation of $d\mathbf{W}$ (Ito or Stratonovitch). Using the Ito-formula [17, 18] we obtain

$$\mathbf{q}_{\text{Ito}}(t, t_0) = \exp\left\{\mathbf{R}\left(\int_{t_0}^{t} d\mathbf{W}_{x,y,z}\right) + (D/2)\mathbf{I}(t - t_0)\right\}\mathbf{q}(t_0) \tag{17}$$

and for the Stratonovich interpretation

$$\mathbf{q}_{\text{Str}}(t, t_0) = \exp\left\{\mathbf{R}\left(\int_{t_0}^{t} d\mathbf{W}_{x,y,z}\right)\right\}\mathbf{q}(t_0) \tag{18}$$

In order to satisfy the identity (15) the Ito interpretation of equation (14) must be excluded as a model of the stochastic quaternion dynamics. Therefore the Stratonovich interpretation (equation (18)) is used to define a finite-difference scheme for the cone model after mapping into the algebra of real quaternions in the vector space $\mathbf{R}^4$ (equation (15)).

We introduce

$$\tilde{\mathbf{R}}(\Delta\mathbf{W}_{x,y,z}) = 2D^{-1/2}(\Delta\mathbf{W}_x^2 + \Delta\mathbf{W}_y^2 + \Delta\mathbf{W}_z^2)^{-1/2}\mathbf{R}(\Delta\mathbf{W}_{x,y,z}) \tag{19}$$

where $\Delta\mathbf{W}_{x,y,z}(t_i, t_{i+1}) = h^{1/2}Z_{x,y,z}$ and $h = t_{i+1} - t_i$ is the time step and $Z_{x,y,z}$ are mutually independent standard gaussian random deviates.

Since

$$\tilde{\mathbf{R}}^2 = -\mathbf{I} \tag{20}$$

we can write the finite-difference version of (18) as

$$\mathbf{q}_{i+1} = \exp\{\tilde{\mathbf{R}}(D^{1/2}/2)(\Delta\mathbf{W}_x^2 + \Delta\mathbf{W}_y^2 + \Delta\mathbf{W}_z^2)^{1/2}\}\mathbf{q}_i \tag{21}$$

and use (20) to calculate the matrix exponential explicitly. The value $\mathbf{q}_{i+1}$ of quaternions at the time step $i + 1$ is expressed through the value $\mathbf{q}_i$ at the time step $i$ as

$$\begin{aligned}\mathbf{q}_{i+1} = [&\mathbf{I}\cos((D^{1/2}/2)(\Delta\mathbf{W}_x^2 + \Delta\mathbf{W}_y^2 + \Delta\mathbf{W}_z^2)^{1/2}) \\ &+ \tilde{\mathbf{R}}\sin((D^{1/2}/2)(\Delta\mathbf{W}_x^2 + \Delta\mathbf{W}_y^2 + \Delta\mathbf{W}_z^2)^{1/2})]\mathbf{q}_i\end{aligned} \tag{22}$$

It is easy to check that (15) and (16) are satisfied identically at each time step provided that (15) and (16) have been satisfied at the previous step.

It is possible to write another finite-difference scheme which is equivalent to (22) up to $(\Delta\mathbf{W}_x^2 + \Delta\mathbf{W}_y^2 + \Delta\mathbf{W}_z^2)^{3/2}$ and which satisfies (15) and (16) identically at every step.

$$\begin{aligned}\mathbf{q}_{i+1} &= [\mathbf{I}(D^{1/2}/2)(1 - \Delta\mathbf{W}_x^2 - \Delta\mathbf{W}_y^2 - \Delta\mathbf{W}_z^2)^{1/2} \\ &\quad + \tilde{\mathbf{R}}(D^{1/2}/2)(\Delta\mathbf{W}_x^2 + \Delta\mathbf{W}_y^2 + \Delta\mathbf{W}_z^2)^{1/2}]\mathbf{q}_i \\ &= [\mathbf{I}(D^{1/2}/2)(1 - \Delta\mathbf{W}_x^2 - \Delta\mathbf{W}_y^2 - \Delta\mathbf{W}_z^2)^{1/2} + \mathbf{R}]\mathbf{q}_i\end{aligned} \tag{23}$$

This scheme is faster from computational point of view.

In order to use trajectories of (14) to compute the correlation functions $K_2$ for restricted motion in distorted and undistorted cones we need rejection rules for the trajectories at the boundary of the cone. Note that the two identities follow from (12):

$$\begin{aligned} e_1^2 + e_2^2 &= \sin(\theta/2)^2 \\ e_0^2 + e_3^2 &= \cos(\theta/2)^2 \end{aligned} \tag{24}$$

It means that the two pairs of quaternion $\{e_1, e_2\}$ and $\{e_0, e_3\}$ cross their respective boundaries (which are circles of radii $|\sin(\theta_b/2)|$ and $|\cos(\theta_b/2)|$, respectively) simultaneously and in opposite direction i.e. when the pair $\{e_1, e_2\}$ comes out of the circle of the radius $|\sin(\theta_b/2)|$ the pair $\{e_0, e_3\}$ comes in the circle of the radius $|\cos(\theta_b/2)|$. The rejection rules for a circle is given in Appendix B.

## 5. THE STEREOGRAPHIC PROJECTION ALGORITHM

In both approaches described in paragraphs 3 and 4 we increased the dimension of the Langevin equations to simulate diffusion on part of the sphere. It allowed us to solve simple and singularity-free equations. We can choose another possibility and use a suitable projection of the relevant part of the sphere into the plane. For this purpose we use the stereographic projection illustrated in Figure 3. Then the part of the sphere restricted by the conditions (2) or (3) is transformed into the circle or ellipse in the $x_1$, $x_2$-plane.

Changing the variables according to

$$\begin{aligned} x &= 2x_1/(1 + x_1^2 + x_2^2)^{-1/2} \\ y &= 2x_2/(1 + x_1^2 + x_2^2)^{-1/2} \\ z &= (x_1^2 + x_2^2 - 1)/(1 + x_1^2 + x_2^2)^{-1/2} \end{aligned} \tag{25}$$

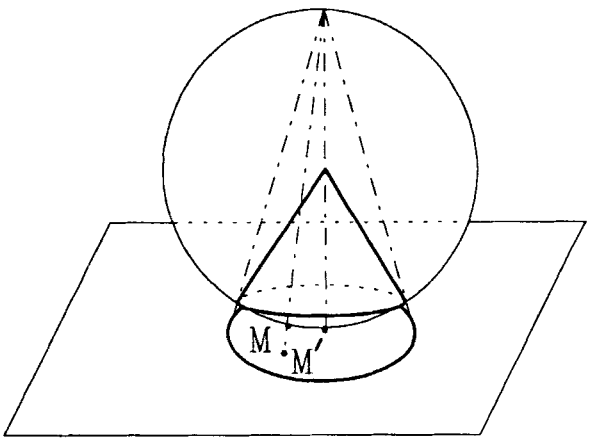


**Figure 3** Stereographic projection. The point $M$ on the surface of the unit sphere is projected into point $M'$ on the plane.

here $x_1$ and $x_2$ are coordinates of the plane, we transform the diffusion equation (1) into

$$\frac{\partial P}{\partial t} = 4^{-1}(1 + x_1^2 + x_2^2)^2 D \Delta_{x_1, x_2} P \tag{26}$$

Stochastic differential equations in Ito form are easily derived:

$$\begin{aligned} dx_1 &= 2^{-1/2}(1 + x_1^2 + x_2^2) D^{1/2} d\mathbf{W}_1 \\ dx_2 &= 2^{-1/2}(1 + x_1^2 + x_2^2) D^{1/2} d\mathbf{W}_2 \end{aligned} \tag{27}$$

The system of equations (27) is singularity free and has the lowest possible dimension 2 (equations for trajectories in the Cartesian coordinates are 3-dimensional and in the quaternion parameterization 4-dimensional). On the other hand noises $(d\mathbf{W}_1, d\mathbf{W}_2)$ enter the system in parametric way and this along with the fact that (27) are Ito differential equations makes the problem of finite-difference approximation a little bit difficult.

For numerical simulations of (27) we have used stochastic version of Runge-Kutta scheme [26] of the second order which for this particular case has the following form

$$x_{1,2}^{i+1} = x_{1,2}^i + D^{1/2} \Delta \mathbf{W}_{1,2}^0 g\,(x_1^i + 2^{-1/2} \Delta \mathbf{W}_1^1 g\,(x_1^i, x_2^i),\ x_2^i + 2^{-1/2} \Delta \mathbf{W}_2^1 g(x_1^i, x_2^i)) \tag{28}$$

where $g(x_1, x_2) = 2^{1/2}(1 + x_1^2 + x_2^2)$; $\Delta \mathbf{W}_{1,2}^{0,1} = h^{1/2} Z_{1,2}^{0,1}$; $h$ is the time step and $Z_{1,2}^{0,1}$ are four mutually independent standard gaussian random deviates.

The rejection rules for trajectories of (27) on the boundary defined by (2) or (3) are described in Appendix B.

## 6. SIMULATION OF CORRELATION FUNCTION $K_2$ FOR THE DISTORTED CONE

In this section we present a number of illustrative calculations of the correlation function $K_2$ for the undistorted cone (Figure 4) and compare them with $K_2$ plots for several cone distortions (see Figure 5). Figures 6–8 show $\ln(K_2^R)$ after subtraction of the plateau value and a renormalization:

$$K_2^R(t) = \frac{K_2(t) - \text{plateau}}{K_2(0) - \text{plateau}} \tag{29}$$

From Figure 5 we can see that the most pronounced effect of the distortion is an increase of the plateau value. This is quite understandable since distortion of the cone reduces the part of the unit sphere where the unit vector is allowed to diffuse. The relaxation properties have a more complicated behavior. According to the results for undistorted cone shown in Figure 6 and 8 we can divide the range of $\theta_b - [0, \pi]$ - into three region with respect to qualitatively different behavior of $K_2$. In the interval approximately $0 < \theta_b < \pi/4$ $K_2^R$ is characterized by a single exponential (Figure 6). In $\pi/4 < \theta_b < 3\pi/4$ multiexponentiality becomes more

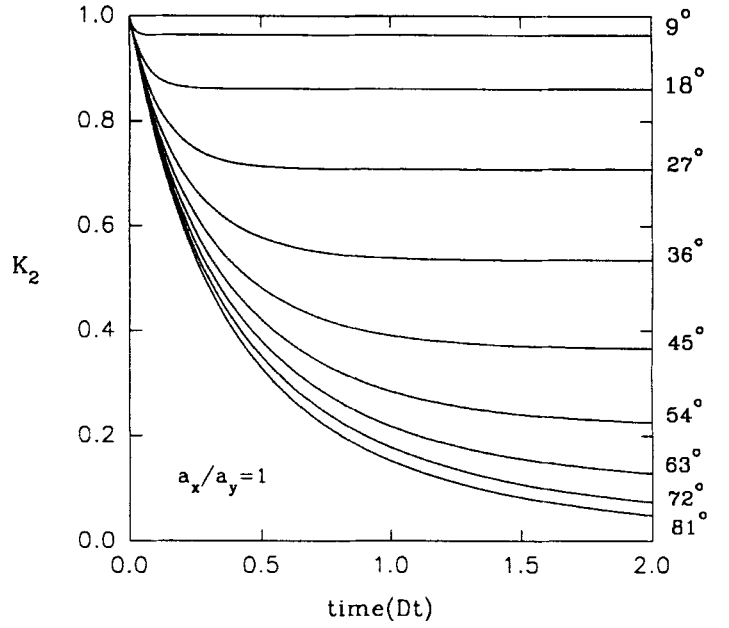


**Figure 4** A family of correlation function $K_2$ for undistorted cone for different values of cone angle $\theta_b < \pi/2$.

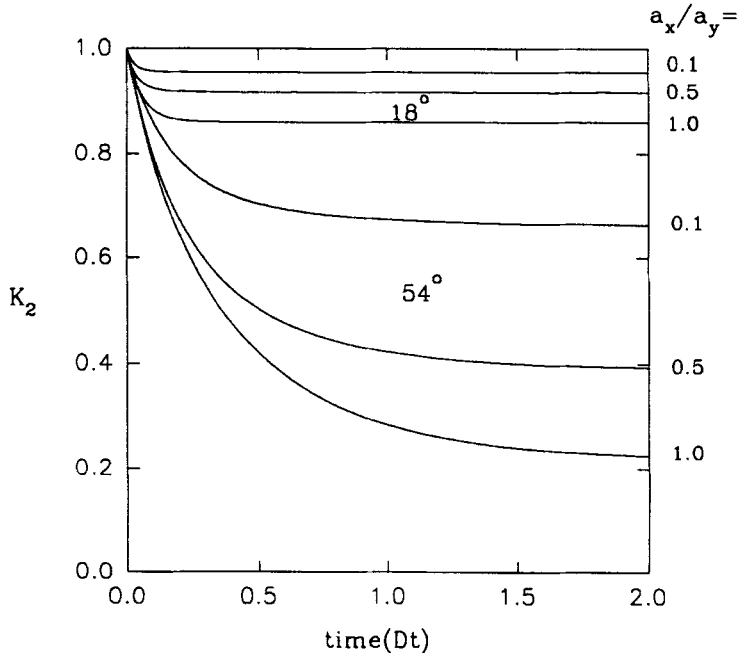


**Figure 5** Effect of cone distortion on $K_2$ for several cone angles $\theta_b < \pi/2$.

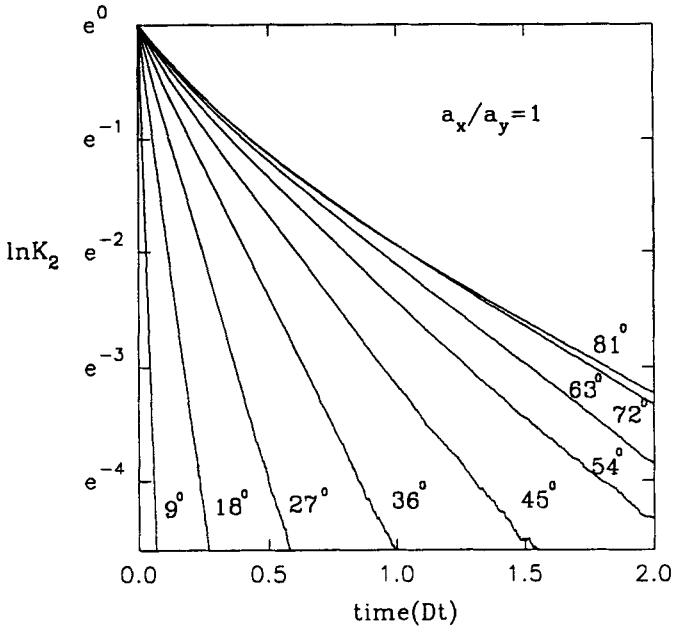


**Figure 6** Relaxation rate dependence on cone angle $\theta_b < \pi/2$.

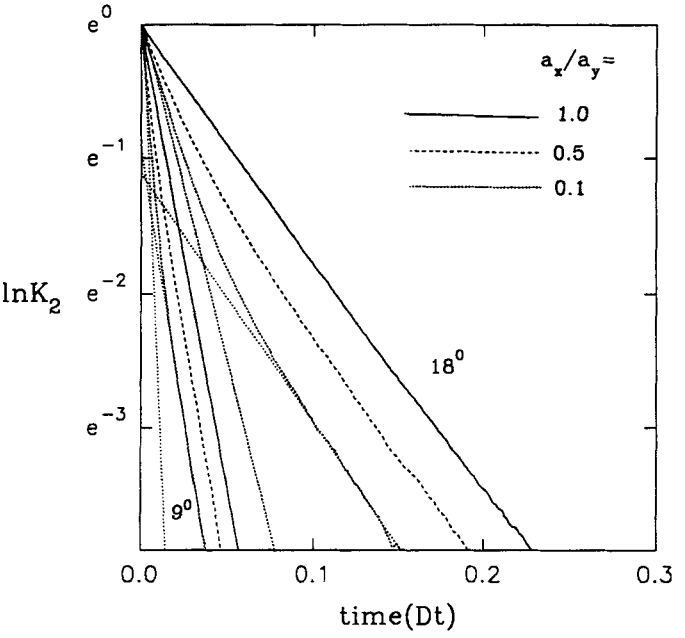


**Figure 7** Effect of cone distortion on relaxation rates of $K_2$ for several cone angles $\theta_b < \pi/2$.

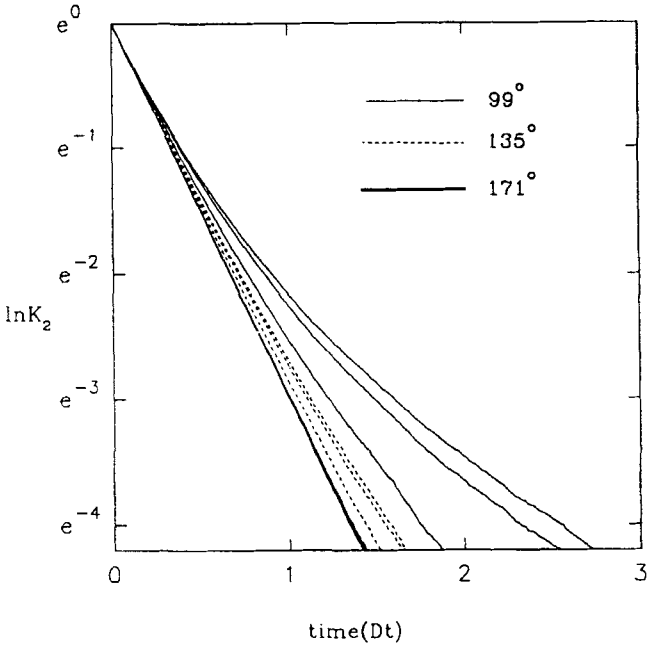


**Figure 8** Relaxation rate dependence on cone angle $\theta_b > \pi/2$ and effect of cone distortion. The curves in each series corresponds to $a_x/a_y = 1$; 0.5; 0.1 top to bottom.

and more pronounced as $\theta_b$ increases. Finally after $3\pi/4$ the relaxation of $K_2^R$ is again very close to single exponential (Figure 8). Note also that the relaxation rate as a function of $\theta_b$ behaves differently in different parts of the $\theta_b$-interval – the relaxation rate decreases with $\theta_b$ from 0 to $\theta_b = \pi/2$ and then increases with $\theta_b$ in $[\pi/2, \pi]$. This behavior is correlated with complicated behavior of the plateau level (exact formula (73) from [2]).

Figures 5, 7 and 8 display the effect of the distortion of the cone on the relaxation rate and the plateau level. For $\theta_b$ in the interval $\theta_b \leq \pi/2$ the distortion induce multiexponentiality in the correlation function. The plateau level increases. This is expected since the deformation of the symmetric cone decrease the available angular space. For $\theta_b > \pi/2$ the distortion procedure is accomplished by changing the ratio of long and short axis of the complementary cone. The distortion of the cone leads to an increase of the surface available for the diffusion of the unit vector. Thus the relaxation rate becomes more single exponential and the plateau first increase and then decreases [2].

## 7. COMPARISON OF NUMERICAL PROPERTIES

In Table 1 we compare the most important features of the three above mentioned algorithms. The algorithms were realized in FORTRAN and run on HP730 workstation. Maximal error has been calculated from comparison with $K_2$ calculated using the eigenfunction expansion [2, 9] which we consider as exact.

**Table 1** Comparative results for Cartesian approach, quaternion parameterization and stereographic projection algorithm $a_x/a_y = 1$; number of trajectories = $10^5$; length of a trajectory = $10^3$ points

| | *Time of calculation* | | *Maximal error* ($\theta = 81^0$) | |
|---|---|---|---|---|
| | $\theta = 9^0$ | $\theta = 81^0$ | *step* = $10^{-2}$ | *step* = $10^{-3}$ |
| Cartesian | 1:53 | 1:21 | $4.8 \cdot 10^{-3}$ | $3.0 \cdot 10^{-3}$ |
| Quaternion* | 2:04 | 1:28 | $4.8 \cdot 10^{-3}$ | $3.7 \cdot 10^{-3}$ |
| Stereographic | 1:19 | 0:56 | $1.37 \cdot 10^{-2}$ | $7.2 \cdot 10^{-3}$ |

* obtained with the scheme (22)

From Table 1 we see that the Stereographic projection algorithm is faster than the other two. The quaternion algorithm needs the largest amount of CPU. The accuracy for the same number of trajectories is best for the Cartesian algorithm and becomes worst for the Stereographic algorithm. In Figures 9–11 the computational error as a function of time is displayed for all three algorithms. The convergency rate of the algorithms agrees with the general estimation for Monte Carlo algorithms - const $N^{-1/2}$ where $N$ is the number of trajectories.

## 8. CONCLUSION

In this paper we have presented three different approaches to simulate Brownian dynamics and used them to calculate correlation functions of second rank spherical

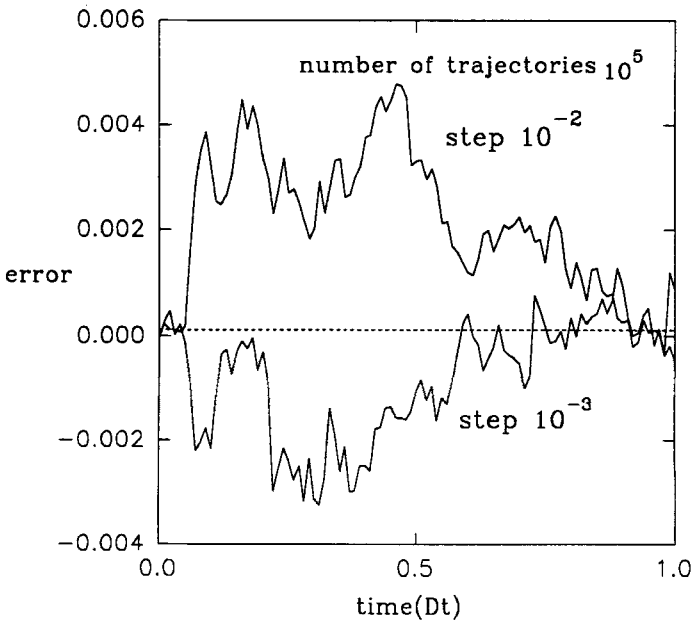


**Figure 9** Dynamic of computational error for the Cartesian algorithm.

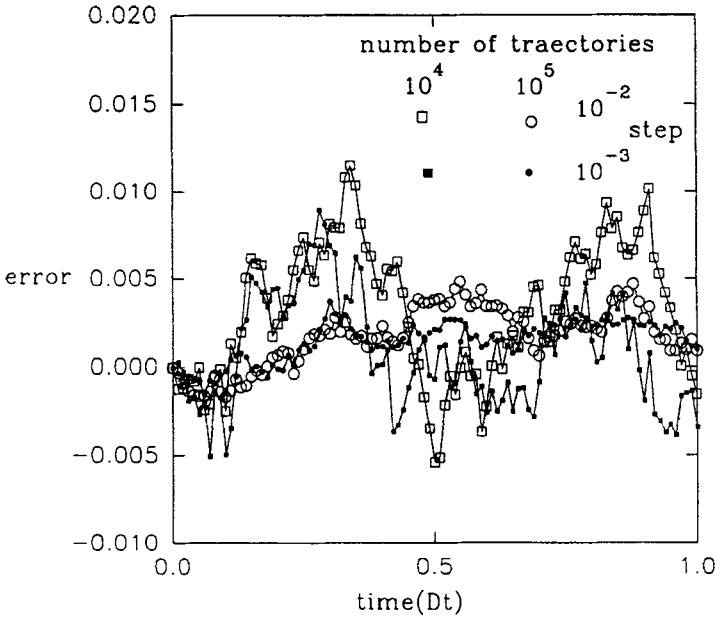


**Figure 10** Dynamic of computational error for the quaternion parameterization algorithm.

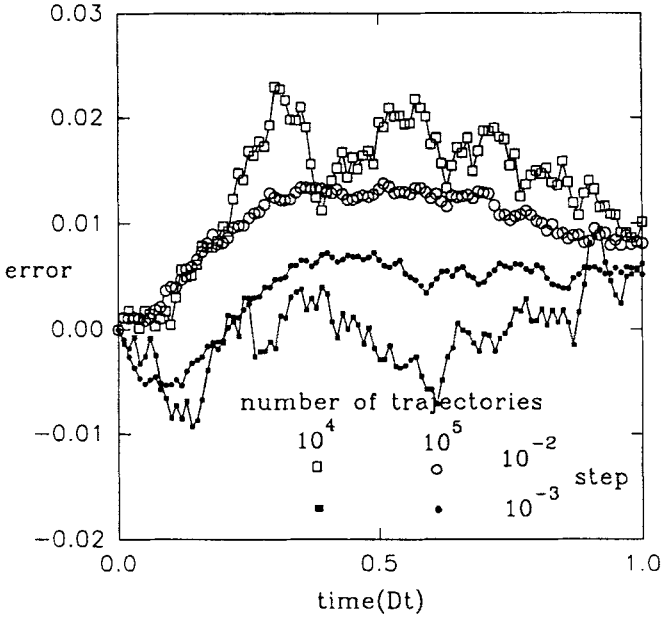


**Figure 11** Dynamic of computational error for the stereographic projection algorithm.

harmonics for the distorted and undistorted cone model. The comparative results of section 7 show that the Cartesian approach is the best one in the sense that it gives the best precision for equal amount of trajectories although it is slower than the Runge-Kutta scheme of the stereographic projection.

We believe, however, that the scope of future applications of the algorithms can be different. As far as the Cartesian and the stereographic projection methods can easily be generalized for diffusion on general and complicated manifolds they are hardly useful for calculations of rotational correlation functions of rigid and flexible molecules where translational and rotational degree of freedom are strongly coupled. For the latter case quaternion parameterization seems to be the only realistic alternative.

*Acknowledgements*

This work was supported by Swedish Natural Science Research Council. One of us (I.F.) gratefully acknowledges the Mat-Nat Faculty of Umeå University for hospitality and financial support.



## APPENDIX A. REJECTION RULES FOR TRAJECTORIES IN CARTESIAN COORDINATES

We consider the Brownian motion which takes place inside the cone with the boundary (c.f. section 2)

$$z^2 = k^2(x^2/a_x^2 + y^2/a_y^2) \tag{A1}$$

where $k^2 = ctn^2\,\theta_0$ and $a_x/a_y$ defines the distortion of the cone. Until a trajectory hits the boundary (Al) it evolves according equation (9). After this event it must be rejected with the same angle to the normal to (Al) erected in the point where the trajectory has crossed the boundary. In finite-difference realization a trajectory (11) consists of joint intervals. Let us define the point before a trajectory has crossed the boundary as $\mathbf{r}_0 = \{x_0, y_0, z_0\}$ and the first point after crossing as $\mathbf{r}_1 = \{x_1, y_1, z_1\}$. Then it is possible to find coordinates of the crossing point using equation (A1)

$$\mathbf{r}_c = \{\Delta x_c + x_0,\ \Delta y_c + y_0,\ \Delta z_c + z_0\} = \{\Delta z_c h_{xz} + x_0\,\Delta z_c h_{yz} + y_0\,\Delta z_c + z_0\} \tag{A2}$$

where

$$\begin{aligned}\Delta z_c = {} & (z_0/k^2 - x_0 h_{xz}/a_x^2 - y_0 h_{yz}/a_y^2 \\ & \mp \{[(x_0 - z_0 h_{xz})^2/a_x^2 + (y_0 - z_0 h_{yz})^2/a_y^2]/k^2 \\ & - (h_{xz}y_0 - h_{yz}x_0)^2/a_x^2 a_y^2\}^{1/2}/[h_{xz}^2/a_x^2 + h_{yz}^2/a_y^2 - 1/k^2]\end{aligned} \tag{A3}$$

and

$$h_{xz} = (x_1 - x_0)/(z_1 - z_0);\ h_{yz} = (y_1 - y_0)/(z_1 - z_0)$$

A rejection point which satisfy the condition "incident angle is equal to rejection angle" is situated at the same distance from the tangent plane to the surface (A1)

at point $\mathbf{r}_c$ but from the other side. So, if we take into account that the equation of the tangent plane is

$$k^2x_c(x - x_c)/a_x^2 + k^2y_c(y - y_c)/a_y^2 - z_c(z - z_c) = 0 \qquad \text{(A4)}$$

then coordinates of the rejection point can be written in a parametric form

$$\mathbf{r}_r = \{x_r, y_r, z_r\} = \{x_1 + 2x_ck^2t/a_x^2;\ y_1 + 2y_ck^2t/a_y^2;\ z - 2z_ct\} \qquad \text{(A5)}$$

where

$$t = (z_cz_1 - k^2x_cx_1/a_x^2 - k^2y_cy_1/a_y^2)/(z_c + k^2x_c/a_x^4 + ky_c/a_y^4) \qquad \text{(A6)}$$

is the distance of $\mathbf{r}_1$ from the tangent plane.

When calculations are carried on with finite steps a situation can be met (shown in Figure 1A) where after the rejection a trajectory still stays outside the cone (A1). This problem can be solved iteratively choosing in every step $\mathbf{r}_c$ as $\mathbf{r}_0$ and repeating the calculations. The logic which is necessary to sort out all such cases makes this part of algorithm very complicated.

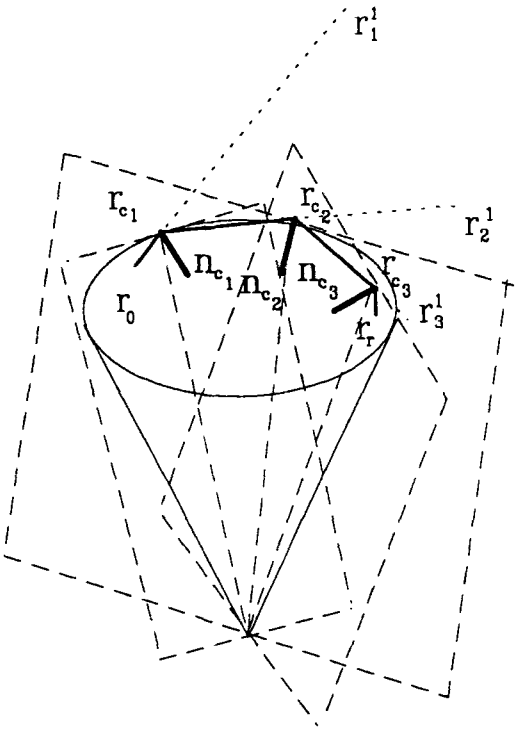


**Figure 1A** Rejection rules for the Cartesian approach. An illustration of the case where random step size is so big that one need three consecutive iterations to return the trajectory back to the cone.

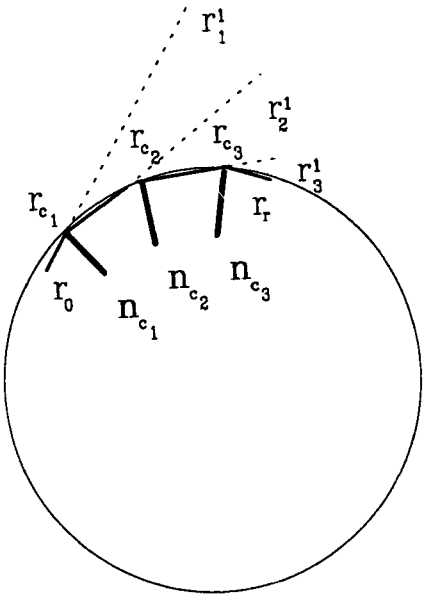


**Figure 1B** Rejection rules for the trajectory of Langevin equations (27) in the stereographic projection approach. An illustration of the cases where the random step size is so big that one needs three iterations to return the trajectory back to the circle.



## APPENDIX B. REJECTION RULES FOR TRAJECTORIES ON THE PLANE

The part of the sphere restricted by the condition (3) is mapped by stereographic projection into elliptic domain on the plane (Figure 1B). Until a trajectory hits the boundary

$$x^2/a_x^2 + y^2/a_y^2 = r^2 \tag{B1}$$

it evolves according to Langevin equation (14) or (27). Let us define as

$$\mathbf{r}_0 = \{x_0, y_0\} \tag{B2}$$

the value of the trajectory at the last step before it crosses the boundary and as

$$\mathbf{r}_1 = \{x_1, y_1\} = \{x_0 + \Delta x_1, y_0 + \Delta y_1\} \tag{B3}$$

the value immediately after.

In order to satisfy boundary condition (3) we must reject the trajectory with the same angle as it hits the boundary. It means that the trajectory is rejected perpendicular to the tangent line, the distance of $\mathbf{r}_r$ from the tangent line being equal to the distance of $\mathbf{r}_1$ from this line.

We find coordinates of the crossing point $\mathbf{r}_c$

$$\mathbf{r}_c = \{x_0 + h_{xy}\Delta y_c;\ y_0 + \Delta y_c\} \tag{B4}$$

where $h_{xy} = \Delta x_1 / \Delta y_1$ and

$$\Delta y_c = [\mp([h_{xy}^2/a_x^2 + 1/a_y^2]r^2 - (x_0 - h_{xy}y_0)^2/a_x^2a_y^2)^{1/2} - h_{xy}x_0/a_x^2 - y_0/a_y^2]/(h_{xy}^2/a_x^2 + 1/a_y^2) \quad \text{(B5)}$$

Then

$$\mathbf{r}_r = \mathbf{r}_1 + 2t\,\mathbf{r}_c \quad \text{(B6)}$$

where

$$t = 1 - \mathbf{r}_c\mathbf{r}_1/r^2 \quad \text{(B7)}$$

is the distance from the point $\mathbf{r}_1$ to the tangent line through the crossing point $\mathbf{r}_c$.

## *References*


[1] K. Kinosita, S. Kawato and A. Ikegami, "A Theory of Fluorescence Polarization Decay in Membranes", *Biophys. J*, **20**, 289 (1977).

[2] C.C. Wang and R. Pecora, "Time-correlation Function for Restricted Rotational Diffusion", *J. Chem. Phys.*, **72**, 5333 (1980).

[3] A. Kumar and G.C. Levy, "Correlation Functions for Restricted Rotational Diffusion of Articulated Bodies", *J. Chem. Phys.*, **85**, 485 (1986).

[4] A. Kumar, "Restricted Rotational Diffusion of Rigid Bodies", *J. Chem. Phys.*, **91**, 1232 (1989).

[5] J. Kowalewski, L. Nordskiöld, N. Benetis and P.-O. Westlund, "Theory of Nuclear Spin Relaxation in Paramagnetic Systems in Solution", *Progr. in NMR Spectrosc.*, **17**, 141 (1985).

[6] Z. Liang and P.-O. Westlund, "ESR Slow-Motion Line Shape for Spin-Labelled Molecules Undergoing Rotational Diffusion in a Cone. Application to Lyso Lecithin/Water Systems". To be published in *J. Chem. Phys.* 1993.

[7] G. Lipari and A. Szabo, "Effect of Librational Motion on Fluorescence Depolarization and Nuclear Magnetic Resonance Relaxation in Macromolecules and Membranes", *Biophys. J.*, **30**, 489 (1980).

[8] G. Lipari and A. Szabo, "Padé Approximants to Correlation Functions for Restricted Rotational Diffusion", *J. Chem. Phys.*, **75**, 2971 (1981).

[9] J.R. Branard and A. Szabo, "Theory for Nuclear Magnetic Relaxation of Probes in Anisotropic Systems: Application to Cholesterol in Phospholipids Vesicles", *Biochemistry*, **20**, 4618 (1981).

[10] B. Halle, S. Ljunggren and S. Lidin, "Theory of Spin Relaxation in Bicontinuous Cubic Liquid Crystals", *J. Chem. Phys.*, **97**, 1401 (1992).

[11] P.-O. Westlund and H. Wennerström, "Electronic Energy Transfer in Liquids. The Effect of Molecular Dynamics", Submitted to *J. Chem. Phys.* (1992).

[12] J. Freed, "Theory of Slow Tumbling ESR Spectra for Nitroxides", in Spin Labelling, ed. L. Berliner, Academic Press, N.Y., 1976.

[13] D.J. Schneider and J. Freed, "Spin Relaxation and Motional Dynamics", *Adv. Chem. Phys.*, **LXXIII**, 387 (1989).

[14] B.H. Robinson, L.J. Slutsky and F.P. Auteri, "Direct Simulation of Continuous Wave Electron Paramagnetic Resonance Spectra from Brownian Dynamic Trajectories", *J. Chem. Phys.*, **96**, 2609 (1992).

[15] P.-O. Westlund and T.P. Larsson, "Proton-Enhanced Relaxation in Low Paramagnetic Complexes (S = 1): Beyond the Solomon-Bloembergen and Morgan Theory. 1. The Smoluchowsky Distortion Model of the ZFS Interaction", *Acta Chemica Scand.*, **45**, 11 (1991).

[16] P.-O. Westlund, T.P. Larsson, and O. Teleman, "Paramagnetic Enhanced Proton Spin-Lattice Relaxation in The $Ni^{2++}$ Hexa Aquo-complexes", To be published in *Mol. Phys.* (1993).

[17] C.W. Gardiner, Handbook of Stochastic Methods, Springer-Verlag, 1985.

[18] B. Øksendal, Stochastic Differential Equations, Springer-Verlag, 1992.

[19] N.G. van Kampen, "Brownian Motion on a Manifold", *Journ. Stat. Phys.*, **44**, 1 (1986).

[20] S. Chandrasekhar, "Stochastic Problems in Physics and Astronomy", *Rev. Mod. Phys.*, **15**, 1 (1943).

[21] I.I. Gikhman, A.V. Skhorohod, Stochastic Differential Equations, Springer-Verlag, 1972.

[22] D.J. Evans, "On the Representation of Orientation space", *Molecular Physics*, **34**, 317 (1977).
[23] D.J. Evans, S. Murad, "Singularity Free Algorithm for Molecular dynamics Simulation of Rigid Polyatomics", *Molecular Physics*, **34**, 327 (1977).
[24] R.M. Lynden-Bell, A.J. Stone, "Reorientational Correlation Functions, Quaternions and Wigner Rotation Matrices" *Molecular Simulation*, **3**, 271 (1989).
[25] S. Engström, M. Lindberg, L. Johansson, "Fluorescence Anisotropy of Rotating Molecules in the Presence of Energy Migration" in PhD thesis by M. Lindberg, Umeå University, 1991.
[26] J.R. Klauder and W.P. Petersen, "Numerical Integration of Multiplicative-Noise Stochastic Differential Equations", SIAM *J. Numer. Anal.*, **22**, 1153 (1985).